The Actin-Based Motor Myosin Vb Is Crucial to Maintain Epidermal Barrier Integrity

Marie Reynier, Sophie Allart, Dominique Goudounèche, Alain Moga, Guy Serre, Michel Simon, Corinne Leprince

THE ACTIN-BASED MOTOR MYOSIN Vb IS CRUCIAL TO MAINTAIN THE EPIDERMAL BARRIER INTEGRITY

Marie Reynier°, Sophie Allart*, Dominique Goudounèche[^], Alain Moga[#], Guy Serre°, Michel Simon° and Corinne Leprince°^.

° UDEAR, UMR 1056 Institut National de la Santé et de la Recherche Médicale, University of Toulouse, Toulouse, France;

* CPTP, UMR 1043 Institut National de la Santé et de la Recherche Médicale, TRI Genotoul, Toulouse, France;

[^] CMEAB, Faculté de Médecine Rangueil, University of Toulouse, Toulouse, France ;

[#] SYNELVIA, Labège, France.

^Corresponding author: Corinne Leprince, UDEAR UMR1056 INSERM, Université de Toulouse, CHU Purpan, Place du Dr Baylac TSA 40031, 31059 Toulouse cedex 09, France.

E-mail: corinne.leprince@inserm.fr

Abbreviations: Cer, ceramide; Ctrl, Control; CDSN, corneodesmosin; DAPI, 4′,6-Diamidine-2′-phenylindole dihydrochloride; GTP, guanosine triphosphate; GTPase, GTP hydrolase; KLK, kallikrein; LB, lamellar bodies; Myo, myosin; RHE, reconstructed human epidermis; shRNA, short hairpin RNA; STED, stimulated emission depletion; SC, stratum corneum; TEER, trans-epithelial electric resistance; TEM: transmission electron microscopy; TEWL, trans-epidermal water loss; TJ, Tight Junction; TGN, Trans Golgi Network.

ABSTRACT

Myosin Vb (Myo5b) is an unconventional myosin involved in the actin-dependent transport and tethering of intracellular organelles. In the epidermis, granular keratinocytes accumulate cytoplasmic lamellar bodies (LB), secretory vesicles released at the junction with the stratum corneum which participate actively in the maintenance of the epidermal barrier. We have previously demonstrated that LB biogenesis is controlled by the Rab11a GTPase, known for its ability to recruit the Myo5b motor. In order to better characterize the molecular pathway that controls LB trafficking, we analyzed the role of F-actin and Myo5b in the epidermis. We demonstrated that LB distribution in granular keratinocytes was dependent on a dynamic F-actin cytoskeleton. Myo5b was shown to be highly expressed in granular keratinocytes and associated with corneodesmosin-loaded LB. In reconstructed human epidermis, Myo5b silencing led to epidermal barrier defects associated with structural alterations of the stratum corneum and a reduced pool of LB showing signs of disordered maturation. Myo5b depletion also disturbed the expression and distribution of both LB cargoes and junctional components such as claudin-1, which demonstrates its action on both LB trafficking and junctional complex composition. Altogether, our data reveal the essential role of Myo5b in maintaining the epidermal barrier integrity.

INTRODUCTION

In the epidermis, the outermost living cell layer is composed of highly differentiated granular keratinocytes which play a crucial role in the maintenance of the epidermal barrier (Elias et al., 1998, Madison, 2003). First, granular keratinocytes have the capacity to assemble tight junction (TJ) complexes, essential for regulating the transit of small molecules across the epithelium (Brandner, 2016). Second, they are secretory cells containing cytoplasmic vesicles called lamellar bodies (LB) (Feingold, 2007; Schmitz and Muller, 1991). LB contain lipid precursors and lipid-modifying enzymes, structural proteins such as corneodesmosin (CDSN), proteases such as kallikreins (KLK), anti-bacterial peptides, etc. All these components are intended to be released by exocytosis in order to fill the intercorneocyte spaces of the stratum corneum (SC).

In a previous report, we demonstrated that the biogenesis of LB is regulated by Rab11a, which belongs to the guanosine triphosphate hydrolase (GTPase) Rab family (Reynier et al., 2016). In three-dimensional *in vitro* reconstructed human epidermis (RHE), Rab11a silencing generated epidermal barrier defects due to an impaired LB pool and drastic changes in the composition of the SC. In skin granular keratinocytes where it is particularly abundant and detected on the surface of LB, Rab11a is believed to control the biogenesis of pre-LB emerging from the Trans Golgi Network (TGN) and maturing along a secretory pathway. However, the molecular cascade that leads to LB exocytosis at the apical plasma membrane of granular keratinocytes remains to be fully characterized.

Rab11a effectors have been clearly identified in various cell types and tissues: most of them are elements of the trafficking machinery (Hales et al., 2002; Cullinane et al., 2010; Roland et al., 2011; Welz et al., 2014; Gruber et al., 2017). In polarized epithelial cells such as small intestine enterocytes (Sobajima et al., 2014) or bladder epithelium umbrella cells (Wankel et al., 2016), the partnership between Rab11a and the actin-based motor myosin 5b (Myo5b)

plays a crucial role in the regulation of apical trafficking. Mutations in the *MYO5B* gene cause a very severe intestinal disorder with life threatening diarrhea (Müller et al., 2008; Ruemmele et al., 2010) called Microvillus Inclusion Disease (MVID; OMIM #251850). Furthermore, a number of studies have revealed that exocytosis of secretory vesicles requires an active F-actin cytoskeleton in multiple subcellular compartments, beyond the TGN exit sites (Guttierez and Villanueva, 2018). First, F-actin fibers may supplement microtubules as long distance tracks, facilitating vesicle motility towards the cortical sites (Schuh, 2011; Pylypenko et al., 2016). Second, cortical actin at the cell periphery plays a scaffolding role for the exocytic machinery and its regulators. Third, F-actin acts as a driving force during the exocytic process at the plasma membrane.

In this study, in order to decipher the molecular basis of trafficking pathways that control the epidermal barrier, we analyzed the importance of the F-actin cytoskeleton and the molecular motor Myo5b, in the epidermis. Disruption of the F-actin cytoskeleton by drug treatment was shown to modify LB distribution in the cytoplasm of granular keratinocytes. In normal epidermis, Myo5b could associate with corneodesmosin loaded structures which are likely to be LB. In RHE, Myo5b silencing induced severe defects of the SC, decreased LB density and modified the expression of LB cargoes and junctional components. From these results, we hypothesize that the molecular motor Myo5b regulates F-actin-dependent vesicular trafficking which ultimately controls the epidermal barrier.

RESULTS

LB distribution is dependent on the F-actin cytoskeleton in granular keratinocytes

In order to study the molecular basis of LB trafficking in the epidermis, we first investigated the importance of the F-actin cytoskeleton through latrunculin treatment, a drug that affects actin polymerization. On tissue sections from drug-treated RHE, the LB cargoes CDSN and KLK7 were less concentrated on the apical side of granular keratinocytes and showed a more dispersed distribution in the cytoplasm compared to control RHE (Figure 1a). These data were strengthened by whole-mount imaging of RHE which substantially improved the detection and 3D analysis of fluorescent signals, i.e. actin and CDSN. The images presented in Figure 1b are Z sections of flattened granular keratinocytes (Yokouchi et al., 2016) and corresponding videos are shown in supplementary material. The CDSN LB marker was present in the whole cell body including the cell edges in control conditions, when it was more localized in the cell center, on larger punctate structures, after latrunculin treatment (highlighted in boxes 1-4, Figure 1c). This suggests that a dynamic F-actin cytoskeleton is important for LB positioning in granular keratinocytes. A possibility is that an actin-based motor might control LB trafficking.

Actin-based Myo5b is associated with LB markers in granular keratinocytes

It has been previously shown that after TGN exit, LB carry the Rab11a GTPase known for its regulatory role in vesicular trafficking (Reynier et al., 2016; Ishida-Yamamoto et al., 2018). Among Rab11a effectors, one of the most frequently reported is the actin-based molecular motor, Myo5b. The expression of *MYO5B* mRNA was analyzed in distinct keratinocyte populations separated as previously described by Toulza et al., 2007. The ratio between granular and basal cells was 23.63 ± 12.26 indicating an increasing expression gradient along

with keratinocyte differentiation. Such a gradient was not found for another member of the Myo5 family displaying Rab11a binding capacities, *MYO5A* (mRNA ratio of 1.37 ± 0.03). On epidermal sections, the Myo5b protein showed a strong wavy signal at the apical side of granular keratinocytes, a signal which is reminiscent of Rab11a, when Myo5a was homogenously present in the entire epidermis (Figures S1a and S1e). In these cell layers, Myo5b and Rab11a could be found in the same subcellular compartment (Figure S1b). Moreover, Myo5b expression in RHE was reduced after Rab11a silencing, when Myo5a expression was not affected (Figure S1c, d, e). Altogether, these results highlight the possibility of a Rab11a-Myo5b partnership in the cytoplasm of granular keratinocytes.

Thereafter, we examined the distribution of Myo5b along with LB markers in native epidermis. In the outermost granular cell layers, Myo5b partially co-localized with CDSN as well as KLK7 (Figure 2a). By using super-resolution confocal microscopy (STED), Myo5b and CDSN signals were more specifically analyzed and revealed co-localization on punctate structures with a diameter of 100 to 140 nm (see enlarged boxes 1 and 2 in Figures 2b and 2c). When the diameter of the co-labelled structures was calculated on a larger picture (Figure 2b, Merge), it was evaluated at 108 ± 58 nm, which is totally consistent with the known size of LB. The Pearson's coefficient of the two fluorochromes was evaluated as r=0.708, which revealed a significant co-localization between Myo5b and CDSN. These data suggest that Myo5b may associate with cytoplasmic structures which on the basis of their size as well as CDSN labelling are likely to be LB. This association may be dependent on a molecular recruitment by the Rab11a GTPase.

Myo5b silencing induces functional and structural defects in the epidermis

In order to analyze the functional relevance of Myo5b in the epidermis, we performed RNA interference in RHE. Two shRNA that specifically target the *MYO5B* mRNA induced a

consistent inhibition of *MYO5B* expression compared to the non-targeting shRNA control (sh*CTRL*): 76 ± 15% for sh*MYO5B1* and 48 ± 8% for sh*MYO5B2* (Figure S2a). In the same RHE, the expression of *MYO5A* was slightly decreased by sh*MYO5B2* but almost not affected by sh*MYO5B1*. The silencing effect of the sh*RNA*s was confirmed at the protein level (Figure S2b ans S2c).

After hematoxylin-eosin staining, Myo5b-depleted RHE were reproducibly thinner than the controls with a more compact SC, but maintained a normal structure of stratified epithelium, which indicates that keratinocyte differentiation occurred quite normally (Figure 3a). We then investigated the consequences of Myo5b depletion on the functional properties of RHE. First, as a global indicator of barrier tissue integrity, Myo5b-silenced RHE showed decreased trans-epithelial electric resistance (TEER) compared to controls (Figure 3b). Second, in a trans-epidermal water loss (TEWL) assay, Myo5b-depleted RHE demonstrated higher inside-out permeability compared to controls (Figure 3c). Third, in a Lucifer Yellow assay, outside-in permeability was higher after Myo5b silencing and this was most striking with sh*MYO5B1* (Figure 3d). Altogether, these functional assays suggest that Myo5b depletion impairs the barrier function of the epidermis.

These functional data are consistent with substantial alterations of the SC observed by transmission electron microscopy (TEM), after Myo5b silencing. As shown in Figure 4a, corneocytes were tightly packed, inter-corneocyte spaces had almost disappeared and corneocyte matrices were filled with a heterogeneous material that could be remnants of keratinocyte organelles. We performed a quantitative biochemical analysis of major lipids present in the SC, i.e. cholesterol and various types of ceramides, including the ω-acyl ceramides (EOS and EOP) with long carbon chains that are essential for lamella organization. All the types of lipids tested were substantially decreased in the SC after Myo5b depletion (Figure 4b). Since most of the SC lipids are metabolized from lipid precursors transported by

LB, we analyzed the LB pool after Myo5b silencing. In representative electron micrographs shown in Figure 4c, LB (white arrows) were fewer in the cytoplasm of granular keratinocytes compared to control RHE. This difference was confirmed by quantification of LB in a larger series of images where LB density was 0.71 ± 0.37 LB/μm^2 in Myo5b-depleted granular keratinocytes, versus 1.18 ± 0.48 LB/μm^2 in control cells (Figure 4d, upper panel). When LB quantification was restricted to an apical band in granular keratinocytes 1 and 2, as described in supplementary Figure S3, the difference between the 2 groups was even more significant: LB density was 1.74 ± 0.43 LB/μm^2 after Myo5b depletion, versus 2.88 ± 0.92 LB/μm^2 in control conditions (Figure 4d, lower panel). Moreover, it was frequent to find ovoid structures of the same size as LB but with no lamellar content (Figure 4e). These electron-lucent abnormal vesicles could be LB which had undergone a bad maturation. Altogether, our results indicate that the actin-based molecular motor Myo5b regulates the epidermal barrier by controlling the LB cytoplasmic pool, LB maturation along the secretory pathaway and ultimately, the composition and structure of the SC.

Myo5b depletion affects the expression of LB markers and cell junction components

For further examination of the functional properties of Myo5b in the epidermis, we analyzed the consequences of Myo5b depletion on the expression and distribution of critical proteins: (i) LB cargoes such as CDSN and KLK7 and (ii) proteins of junctional complexes such as desmoglein (DSG), E-cadherin and claudin 1 as part of desmosomes, adherens junctions and TJ, respectively. Firstly, once Myo5b was silenced, CDSN and KLK7 had a more dispersed distribution in granular keratinocyte cytoplasm (Figure 5a), and the amount of KLK7 protein detected in a total RHE extract was decreased compared to a control RHE (Figure 5b). Therefore, Myo5b depletion reduced the amount of LB cargoes available in the apical area of granular keratinocytes, which suggests an impairment of LB trafficking. Secondly, Myo5b

silencing decreased the expression of junctional proteins with the highest impact on the TJ component, claudin 1, as shown by western blotting (Figure 5c) or immunostaining of RHE sections (Figure 5d). Such a decrease could impact the TJ structure and function, which are crucial parameters of the epidermal barrier.

DISCUSSION

This work provides evidence that the F-actin cytoskeleton and Myo5b, an actin-based molecular motor, control the epidermal barrier by supporting stages of vesicular trafficking in keratinocytes. We have demonstrated that (i) the F-actin cytoskeleton affects LB distribution in the cytoplasm of granular keratinocytes, (ii) Myo5b is associated with CDSN loaded LB, controls LB trafficking before exocytosis at the SC junction and finally, (iii) Myo5b regulates membrane expression of junctional proteins such as the tight junction component, claudin 1.

The importance of Myo5b in granular keratinocytes is directly related to the previous demonstration that the Rab11a GTPase is essential for LB biogenesis (Reynier et al., 2016). In other tissues, Rab11a has been reported to recruit molecular motors on endosomal vesicles for trafficking regulation along microtubules and actin tracks (Welz et al., 2014). In particular, actin-dependent Myo5b is a major effector of the active Rab11a GTPase (Lapierre et al., 2001; Hales et al., 2002). In mouse oocytes, long-range motility dependent on the actin tracks has been described for Rab11a positive vesicles that are able to recruit Myo5b and actin-nucleation factors (Schuh, 2011). In our RHE model, treatment with an actin-depolymerizing drug tended to maintain larger CDSN-bearing structures in the nuclear periphery. This suggests that actin-dependent transport may apply to LB in granular keratinocytes, just after the TGN exit sites. The flexibility of the actin-based connections between vesicular compartments may facilitate LB maturation through exchange with endosomal compartments. The detection of electron-lucent organelles lacking lamellar content in TEM micrographs of Myo5b-silenced RHE, suggests that the Myo5b molecular motor is crucial for LB maturation. Such atypical LB have also been described in the epidermis of ARC and ARKID patients presenting mutations in the *VPS33B* or *VIPAS39* gene encoding two elements of membrane tethering complexes (Hershkovitz et al., 2008; Rogerson and Gissen, 2018).

In addition, this work shows that Myo5b controls expression and localization of junctional proteins such as the tight junction-associated claudin 1. This is consistent with the decreased TEER and increased TEWL measured on RHE after Myo5b silencing. In the epidermis, the tight junctional complexes are assembled in the penultimate granular keratinocytes, a dynamic process which is linked to cell differentiation and turnover (Rübsam et al., 2017). Our hypothesis is that Myo5b participates in targeting junctional components through endosomal trafficking. When Myo5b is depleted, the endosomal vesicles may be directed towards the degradation compartment, as previously shown in the Rab11a study (Reynier et al., 2016).

The *MYO5B* encoding gene is mutated in MVID, an autosomal recessive disease most frequently characterized by severe diarrhea leading to life-threatening dehydration (Mueller et al., 2008; Ruemmele et al., 2010). This phenotype has been recapitulated in cell line models (Thoeni et al., 2013; Knowles et al., 2014) as well as in KO mice after targeting of the *MYO5B* gene (Carton-Garcia et al., 2015; Schneeberger et al., 2015; Weiss et al., 2016). All these data demonstrate that in enterocytes, Myo5b is a key molecule for the control of apical transport that leads to epithelial cell polarity and function. Despite the ubiquitous expression of Myo5b, *MYO5B* gene mutations have a predominant intestinal impact, with rare cases leading to hepatic cholestasis (Gonzales et al., 2017; Qiu et al., 2017). A targeted study recently performed on a Navajo population of MVID patients reported lighter defects in stomach, liver, kidney and pancreas (Schlegel et al., 2018). These data suggest that *MYO5B* mutations may impact many epithelial tissue types with varying intensities, possibly due to variable mechanisms of compensation. More specifically, the absence of skin defects in MVID patients could be due to the action of another Myo5 isoform, such as Myo5a which is much more expressed in skin tissue than in the small intestine (Roland et al., 2009).

In addition to genetic data, a number of biological studies have documented the importance of Myo5b for apical vesicular trafficking in polarized cells (Roland et al., 2011; Sobajima et al.,

2014; Thoeni et al., 2013; Wankel et al., 2016). In particular, in bladder epithelium umbrella cells, Myo5b controls the transport of uroplakin containing vesicles which emerge from the TGN and undergo exocytosis in response to bladder filling (Khandelwal et al. 2008, 2013). In drosophila photoreceptor cells, Myo5 participates in the transport of rhodopsin-containing vesicles, leading to rhabdomere formation (Li et al., 2007). Therefore, the control of apical vesicle motility by the Myo5b motor is a preserved evolutionary process in polarized cells. Our data show that this process also applies to LB apical trafficking in polarized epidermal keratinocytes.

The diversity of the experimental models mentioned above helped to decipher the molecular basis of the Myo5b-dependent apical trafficking pathway between the TGN exit sites and the exocytic sites. From a proximal Rab11a-Myo5b partnership, these studies identified other players, among which are the Rab8 (Khandelwal et al., 2013; Knowles et al., 2014) and Rab27 GTPases (Wankel et al., 2016), the Myo5a motor and elements of tethering/fusion complexes (Vogel et al., 2015; Knowles et al., 2015). In the epidermis, further studies are necessary to test the relevance of these other trafficking molecules. Since Myo5b is considered to be an anchoring/tethering molecule as much as a motion molecule (Roland et al., 2011), further work is needed to analyze its importance for LB docking at the actin-rich cell cortex.

In conclusion, F-actin and Myo5b control epidermal barrier function through their coordinated action on LB trafficking and membrane targeting of junctional elements. Therefore, along with other epithelia, the ubiquitously expressed Myo5b is shown to have a noteworthy role in the skin.

MATERIALS AND METHODS

Antibodies and reagents

The following antibodies were used: rabbit anti-Myo5b (Sigma-Aldrich, St Louis, MO), rabbit anti-Myo5a (Novus Bio, Littleton, CO), rabbit anti-Rab11a (USBio, Salem, MA), mouse anti-Rab11a (Invitrogen, Carlsbad, CA), mouse anti-CDSN (G36.19 mAb, Serre et al., 1991), goat anti-KLK 6 (R&D systems, Minneapolis, MN), goat anti-KLK 7 (R&D Systems), rabbit anti-claudin 1 (Abcam, Cambridge, UK), mouse anti E-cadherin (BD Biosciences, Franklin Lakes, NJ), mouse anti-desmoglein 1/2 (DG3.10 Progen, Heidelberg, Germany), mouse anti-actin (Millipore, Darmstadt, Germany) and mouse anti-GAPDH (6C5 Santa Cruz Biotech, Dallas, TX). The following secondary antibodies: Alexa Fluor 488 or 555 donkey anti-rabbit IgG, Alexa Fluor 488 or 555 donkey anti-mouse IgG, Alexa Fluor 488 or 555 donkey anti-goat IgG and Alexa Fluor 555 conjugated phalloidin (all from Invitrogen) were used for regular immunofluorescence staining. For STED microscopy, ATTO 594 conjugated anti-mouse IgG and ATTO 647N anti-rabbit IgG were used (Rockland Immunochemicals, Limerick, PA). For western blotting, the following secondary antibodies were used: goat anti-rabbit IgG conjugated to horseradish peroxidase (HRP), swine anti-goat IgG conjugated to HRP (Southern Biotech, Birmingham, AL) and goat anti-mouse IgG conjugated to HRP (Bethyl Laboratories, Montgomery, TX). All reagents were from Sigma Aldrich unless stated.

shRNA lentiviral particles

For RNA silencing in keratinocytes, we used MISSION pLKO.1-puro vector-based lentiviral particles containing a puromycin resistance gene and a shRNA insert under the human U6 promoter (Sigma Aldrich). The shRNA targeting the *RAB11A* mRNA sequence was the same as previously used (Reynier et al., 2016). Two shRNAs that target the *MYO5B* mRNA sequence (NCBI reference NM_001080467) were tested (sh*MYO5B1* and sh*MYO5B2*). In some experiments, only sh*MYO5B1* was used and referred to as sh*MYO5B*. A shRNA that

does not target any known mammalian mRNA sequence was used as a negative control (sh*CTRL*).

Skin samples, keratinocyte populations and RHE

Human abdominal skin samples (from females undergoing plastic surgery, without any history of skin diseases) were obtained from Genoskin (Toulouse, France), following written, informed consent of the donor and as authorized by the French Ministry of Research (#AC-2017-2897). Normal human keratinocyte populations were obtained from epidermal fragments treated with trypsin-EDTA at 4°C and dissociated. For RHE, 350,000 normal human keratinocytes in Epilife medium (Invitrogen) containing 1.5 mmol/l calcium were seeded on polycarbonate culture inserts (area of 0.63 cm^2 with pores of 0.4μm in diameter, Sigma Aldrich). After 48 h of incubation at 37°C in a humidified atmosphere containing 5% CO_2, cells were exposed to the air-liquid interface, and 50 μg/ml vitamin C (Sigma Aldrich) and 10 ng/ml keratinocyte growth factor (KGF, Sigma Aldrich) were added to the medium in the lower compartment. The medium was renewed every 2 days during the 12-day culture at the air-liquid interface (Franckart et al., 2012; Pendaries et al., 2014). Experiments were performed with normal human keratinocytes from 5 individuals.

In order to inhibit the dynamics of actin cytoskeleton, RHE were treated for 2h with Latrunculin A at 0.5 μM versus vehicle (DMSO).

Keratinocyte transduction

Normal human keratinocytes were cultured in complete Dermalife medium (Cellsystems, Troisdorf, Germany) in a humidified atmosphere containing 5% CO2 at 37°C. Keratinocytes were transduced with lentiviral particles containing either sh*CTRL*, sh*RAB11A*, sh*MYO5B1* or sh*MYO5B2* at a multiplicity of infection of 5 in the presence of 6 μg/ml of protamine sulfate (Sigma Aldrich). After 24h of incubation, the culture medium was replaced with fresh

medium containing 2 μg/ml of puromycin (Sigma Aldrich) for selection. After selection, when keratinocytes covered at least 70% of the flask area, they were used to produce RHE as described above.

Statistical analysis

All data are presented as mean ± standard deviation. Statistical differences were determined with student *t* tests. The threshold for statistical significance was set at $p<0.05$.

Further details are available in Supplementary Material.

CONFLICT OF INTEREST

The authors declare no conflict of interest.

ACKNOWLEDGEMENTS

This research was supported by the French National Institute of Health and Medical Research (INSERM), the University of Toulouse and the French Society of Dermatology (SFD). We are indebted to C. Pons for her excellent technical assistance, her suggestions and tremendous contribution to this work. We acknowledge P. Descargues (Genoskin, Toulouse, France) for his help in obtaining skin samples, F. Capilla from the histopathology facility, D. Daviaud and A. Canivet from the imaging facility (Toulouse RIO, University of Toulouse, France). We also thank M. Masson-Regnaut, M.C. Méchin and N. Gaudenzio for their help and advices.

REFERENCES

Bligh EG and Dyer WJ. A rapid method of total lipid extraction and purification. Can J Biochem Physiol 1959;37:911-7.

Bolte S and Cordelières FP. A guided tour into subcellular colocalization analysis in light microscopy. J Microsc 2006;224:213-32.

Brandner JM. Importance of tight Junctions in Relation to Skin Barrier Function. Curr Probl Dermatol 2016;49:27-37.

Carton-Garcia F, Overeem AW, Nieto R, Bazzocco S, Dopeso H, Macaya I et al. *Myo5b* knockout mice as a model of microvillus inclusion disease. Sci Rep 2015;5:12312.

Cullinane AR, Straatman-Iwanowska A, Zaucker A, Wakabayashi Y, Bruce CK, Luo G et al. Mutations in VIPAR cause an arthrogryposis, renal dysfunction and cholestasis syndrome phenotype with defects in epithelial polarization. Nat Genet 2010;42:303-12.

Elias PM, Cullander C, Mauro T, Rassner U, Kömüves L, Brown BE et al. The secretory granular cell: the outermost granular cell as a specialized secretory cell. J Invest Dermatol Symp Proc 1998;3:87-100.

Feingold KR. The role of epidermal lipids in cutaneous permeability barrier homeostasis. J Lipid Res 2007;48:2531-46.

Frankart A, Malaisse J, De Vuyst E, Minner F, de Rouvroit CL, Poumay Y. Epidermal morphogenesis during progressive in vitro 3D reconstruction at the air-liquid interface. Exp Dermatol 2012;21:871-5.

Gonzales E, Taylor SA, Davit-Spraul A, Thébaut A, Thomassin N, Guettier C et al. MYO5B mutations cause cholestasis with normal serum gamma-glutamyl transferase activity in children without microvillous inclusion disease. Hepatol 2017;65:164-73.

Gruber R, Rogerson C, Windpassinger C, Banushi B, Straatman-Iwanowska A, Hanley J, et al. Autosomal recessive keratoderma ichthyosis- deafness (ARKID) syndrome is caused by

VPS33b mutations affecting Rab protein interaction and collagen modification. J Invest Dermatol 2017;137:845-54.

Gutiérrez LM and Villanueva J. The role of F-actin in the transport and secretion of chromaffin granules: an historic perspective. Pflugers Arch 2018;470:181-6.

Hales CM, Vaerman JP, Goldenring JR. Rab11 family interacting protein 2 associates with myosin Vb and regulates plasma membrane recycling. J Biol Chem 2002;22:50415-21.

Hershkovitz D, Mandel H, Ishida-Yamamoto A, Chefetz I, Hino B, Luder A et al. Defective lamellar granule secretion in arthrogryposis, renal dysfunction, and cholestasis syndrome caused by a mutation in VPS33B. Arch Dermatol 2008;144:334-40.

Ishida-Yamamoto A, Igawa S, Kishibe M. Molecular basis of the skin barrier structures revealed by electron microscopy. Exp Dermatol, in press.

Khandelwal P, Ruiz WG, Balestreire-Hawryluk E, Weisz OA, Goldenring JR, Apodaca G. Rab11a-dependent exocytosis of discoidal/fusiform vesicles in bladder umbrella cells. Proc Natl Acad Sci USA 2008;105:15773-8.

Khandelwal P., Prakasam HS, Clayton DR, Ruiz WG, Gallo LI, Van Roekel D et al. A Rab11a-Rab8a-Myo5B network promotes stretch-regulated exocytosis in bladder umbrella cells. Mol Biol Cell 2013;24:1007-19.

Knowles BC, Roland JT, Krishnan M, Tyska MJ, Lapierre LA, Dickman PS et al. Myosin Vb uncoupling from RAB8A and RAB11A elicits microvillus inclusion disease. J Clin Invest 2014;124:2947-62.

Knowles BC, Weis VG, Yu S, Roland JT, Williams JA, Alvarado GS et al. Rab11a regulates syntaxin 3 localization and microvillus assembly in enterocytes. J Cell Sci 2015;126:1616-26.

Lapierre LA, Kumar R, Hales CM, Navarre J, Bhartur SG, Burnette JO et al. Myosin vb is associated with plasma membrane recycling systems. Mol Biol Cell 2001;12:1843-57.

Li BX, Satoh AK, Ready DF. Myosin V, rab11, and dRip11 direct apical secretion and cellular morphogenesis in developing Drosophila photoreceptors. J Cell Biol 2007;4:659-69.

Madison KC. Barrier function of the skin: "la raison d'être" of the epidermis. J Invest Dermatol 2003;121:231-41.

Müller T, Hess MW, Schiefermeier N, Pfaller K, Ebner HL, Heinz-Erian P et al. MYO5B mutations cause microvillus inclusion disease and disrupt epithelial cell polarity. Nat Genet 2008;40:1163-5.

Pendaries V, Malaisse J, Pellerin L, Le Lamer M, Nachat R, Kezic S et al. Knockdown of filaggrin in a three-dimensional reconstructed human epidermis impairs keratinocyte differentiation. J Invest Dermatol 2014;134:2938-46.

Pylypenko O, Welz T, Tittel J, Kollmar M, Chardon F, Malherbe G et al. Coordinated recruitment of Spir actin nucleators and myosin V motors to Rab11 vesicle membranes. Elife. 2016;5. pii: e17523.

Qiu YL, Gong JY, Feng JY, Wang RX, Han J, Liu T et al. Defects in myosin VB are associated with a spectrum of previously undiagnosed low γ-glutamyltransferase cholestasis. Hepatol 2017;65:1655-69.

Reynier M, Allart S, Gaspard E, Moga A, Goudouneche D, Serre et al. Rab11a is essential for lamellar body biogenesis in the human epidermis. J Invest Dermatol 2016;136:1199-209.

Rogerson C and Gissen P. VPS33b and VIPAR are essential for epidermal lamellar body biogenesis and function. Biochem Biophys Acta 2018;1864:1609-21.

Roland JT, Lapierre LA and Goldenring JR. Alternative splicing in class V myosins determines association with Rab10. J Biol Chem 2009;284:1213-23.

Roland JT, Bryant DM, Datt A, Itzen A, Mostov KE, Goldenring JR. Rab GTPase-Myo5B complexes control membrane recycling and epithelial polarization. Proc Natl Acad Sci USA 2011;108:2789-94.

Rübsam M, Mertz AF, Kubo A, Marg S, Jüngst C, Goranci-Buzhala G et al. E-cadherin integrates mechanotransduction and EGFR signaling to control junctional tissue polarization and tight junction positioning. Nat Commun 2017;8:1250.

Ruemmele FM, Müller T, Schiefermeier N, Ebner HL, Lechner S, Pfaller K et al. Loss-of-function of MYO5B is the main cause of microvillus inclusion disease: 15 novel mutations and a CaCo-2 RNAi cell model. Hum Mutat 2010;31:544-51.

Schlegel C, Weis VG, Knowles BC, Lapierre LA, Martin MG, Dickman P et al. Apical membrane alterations in non-intestinal organs in microvillus inclusion disease. Dig Dis Sci 2018;63:356-65.

Schmittgen TD, Livak KJ. Analyzing real-time PCR data by the comparative C(T) method. Nat Protoc 2008;3:1101-8.

Schmitz G and Müller G. Structure and function of lamellar bodies, lipid-protein complexes involved in storage and secretion of cellular lipids. J Lipid Res 1991;32:1539-70.

Schneeberger K, Vogel GF, Teunissen H, Van Ommen DD, Begthel H, El Bouazzaoui L et al. An inducible mouse model of microvillus inclusion disease reveals a role for myosin Vb in apical and basolateral trafficking. Proc Natl Acad Sci USA 2015;112:12408-13.

Schuh M. An actin-dependent mechanism for long-range vesicle transport. Nat Cell Biol 2011;13:1431-6.

Serre G, Mils V, Haftek M, Vincent C, Croute F, Réano A et al. Identification of late differentiation antigens of human cornified epithelia, expressed in re-organized desmosomes and bound to cross-linked envelope. J Invest Dermatol 1991;97:1061-72

Sobajima T, Yoshimura SI, Iwano T, Kunli M, Watanabe M, Atik N et al. Rab11a is required for apical protein localization in the intestine. Biol Open 2014;4:86-94.

Thoeni CE, Vogel GF, Tancevski I, Geley S, Lechner S, Pfaller K et al. Microvillus inclusion disease: loss of myosin Vb disrupts intracellular traffic and cell polarity. Traffic 2013;15:22-42.

Toulza E, Mattiuzzo NR, Galliano MF, Jonca N, Dossat C, Jacob D et al. Large-scale identification of human genes implicated in epidermal barrier function. Genome Biol 2007;8:R107.

Vogel GF, Klee KMC, Janecke AR, Müller T, Hess MW, Huber LA. Cargo-selective apical exocytosis in epithelial cells is conducted by Myo5B, Slp4a, Vamp7, and Syntaxin 3. J Cell Biol 2015;211:587-604.

Wankel B, Ouyang J, Guo X, Hadjiolova K, Miller J, Liao Y et al. Sequential and compartmentalized action of Rabs, SNAREs, and MAL in the apical delivery of fusioform vesicles in urothelial umbrella cells. Mol Biol Cell 2016;27:1621-34.

Weiss VG, Knowles BC, Choi E, Goldstein AE, Williams JA, Manning EH et al. Loss of MYO5B in mice recapitulates microvillus inclusion disease and reveals an apical trafficking pathway distinct to neonatal duodenum. Cell Mol Gastroenterol Hepatol 2016;2:131-57.

Welz T, Wellbourne-Wood J, Kerkhoff E. Orchestration of cell surface proteins by Rab11. Trends Cell Biol 2014;24:407-15.

Yokouchi M, Atsugi T, Van Logtestijn M, Tanaka RJ, Kajimura M, Suematsu M et al. Epidermal cell turnover across tight junctions based on Kelvin's tetrakaidecahedron cell shape. ELife. 2016;5.pii: e19593.

FIGURE LEGENDS

Figure 1. The dynamics of actin cytoskeleton influences LB distribution in granular keratinocytes

(a) DMSO or Latrunculin A-treated RHE sections were stained with anti-CDSN or anti-KLK7 antibody. Scale bars = 10 μm. n≥3. **(b)** RHE were stained as whole-mount samples with anti-CDSN (green), phalloidin (Red), and 4', 6-diamidino-2-phenylindole (DAPI, blue). Images were deconvoluted and analyzed with Imaris software. Subsequent Z sections of a representative granular keratinocyte 2 are presented. Insert boxes in the bottom panels correspond to phalloidin staining in deeper Z sections of the RHE (spinous keratinocytes) to control drug treatment on actin cables. Scale bar = 10 μm. **(c)** Boxes from panel 1b were enlarged. Scale bar = 2 μm.

Figure 2. Actin-based Myo5b is highly expressed in granular keratinocytes and associates with LB

(a) Normal human skin sections were analyzed by confocal microscopy after staining with anti-Myo5b, anti-CDSN, anti-KLK7 and anti-KLK6 antibodies. The image superposition of Myo5b/CDSN, Myo5b/KLK7 and Myo5b/KLK6 are shown in the right panels (Merge) with 4', 6-diamidino-2-phenylindole (DAPI) used as a nuclear counterstain (blue). Scale bars = 10 μm. n≥3. **(b)** A normal skin section was immunostained with an anti-CDSN (green) and anti-Myo5b (red) antibodies. The images were acquired by STED microscopy and were linearly deconvolved with the Huygens software. Scale bar = 1 μm. n≥3. Enlarged views of boxes 1 and 2 are shown. **(c)** Graphs show the signal intensities and the diameter sizes of the co-labelled structures along the lines drawn in high magnification boxes 1 and 2.

Figure 3. Myo5b silencing alters the epidermal barrier

(a) Sections of sh*CTRL* and sh*MYO5B1* RHE were stained with hematoxylin-eosin. A representative experiment is shown, n≥3**.** Scale bar = 10 μm. **(b)** The integrity of sh*CTRL*, sh*MYO5B1* and sh*MYO5B2* RHE was assessed by measuring the trans-epithelial electric resistance (TEER). Data are mean ± SD, n≥3. Unpaired Student's t-test, *** P < 0.001. **(c)** The inside-out epidermal barrier was assessed by measuring trans-epidermal water loss (TEWL) in sh*CTRL*, sh*MYO5B1* and sh*MYO5B2* RHE. Data are mean ± SD, n≥3. Unpaired Student's t-test, *** P < 0.001. **(d)** The outside-in epidermal barrier in sh*CTRL*, sh*MYO5B1* and sh*MYO5B2* RHE was assessed with a Lucifer Yellow penetration assay. Penetration of dye was estimated in the culture medium after 0-24h of incubation at 37°C. Data are mean ± SD, n≥3.

Figure 4. Myo5b silencing alters the structure and composition of the SC, and disrupts LB formation

(a) The SC of sh*CTRL* and sh*MYO5B1* RHE were analyzed by TEM, scale bar = 500 nm. n≥3. **(b)** The level of different lipid species was analyzed in the SC of sh*CTRL* or sh*MYO5B1* RHE: short ceramides Cer-NS, Cer-NP, Cer-AS, Cer-NDS, Cer-ADS (left histogram); acyl-ceramides Cer-EOS and Cer-EOP (middle histogram) and cholesterol (right histogram). Data are mean ± SD, n≥3. Unpaired Student's t-test, *** P < 0.001, ** P < 0.01, * P < 0.05. **(c)** Representative TEM images of sh*CTRL* and sh-*MYO5B1* RHE with a focus on granular keratinocyte 2 in order to analyze LB (white arrows) density, scale bar = 500 nm. **(d)** Quantitative analysis of LB density in the cytoplasm (upper panel) or in an apical area (lower panel, see Supplementary Figure S3) of granular keratinocytes from sh*CTRL* versus sh*MYO5B* RHE, was performed on random electron micrographs. Data are mean ± SD.

Unpaired Student's t-test, * P < 0.05, ** P < 0.01. **(e)** Magnification images of atypical LB-like structures (white arrows) found in sh*MYO5B* RHE compared to sh*CTRL* RHE, scale bar = 100 nm.

Figure 5. *MYO5B* silencing alters the expression and distribution of LB cargoes and junctional components

(a) sh*CTRL* or sh*MYO5B1* RHE sections were stained with anti-Myo5b, anti-Myo5a, CDSN or KLK7 antibody. Scale bars = 10 µm. n≥3. **(b)** Total protein extracts from sh*CTRL* and sh*MYO5B1* RHE were analyzed by western blot using anti-Myo5b, anti-Myo5a, CDSN or KLK7 antibody. Protein extract loading was verified with anti-actin antibody. n≥3. **(c)** Total protein extracts from sh*CTRL* and sh*MYO5B* RHE were analyzed by western blot using anti-Myo5b, anti-DSG 1/2, anti-E-Cadherin or anti-Claudin 1 antibody. Protein extract loading was verified with anti-actin antibody. n≥3. **(d)** sh*CTRL* or sh*MYO5B* RHE sections were stained with anti-Myo5b, anti-DSG 1/2, anti-Claudin 1 or anti-E-Cadherin antibody. Scale bars = 10 µm. n≥3.

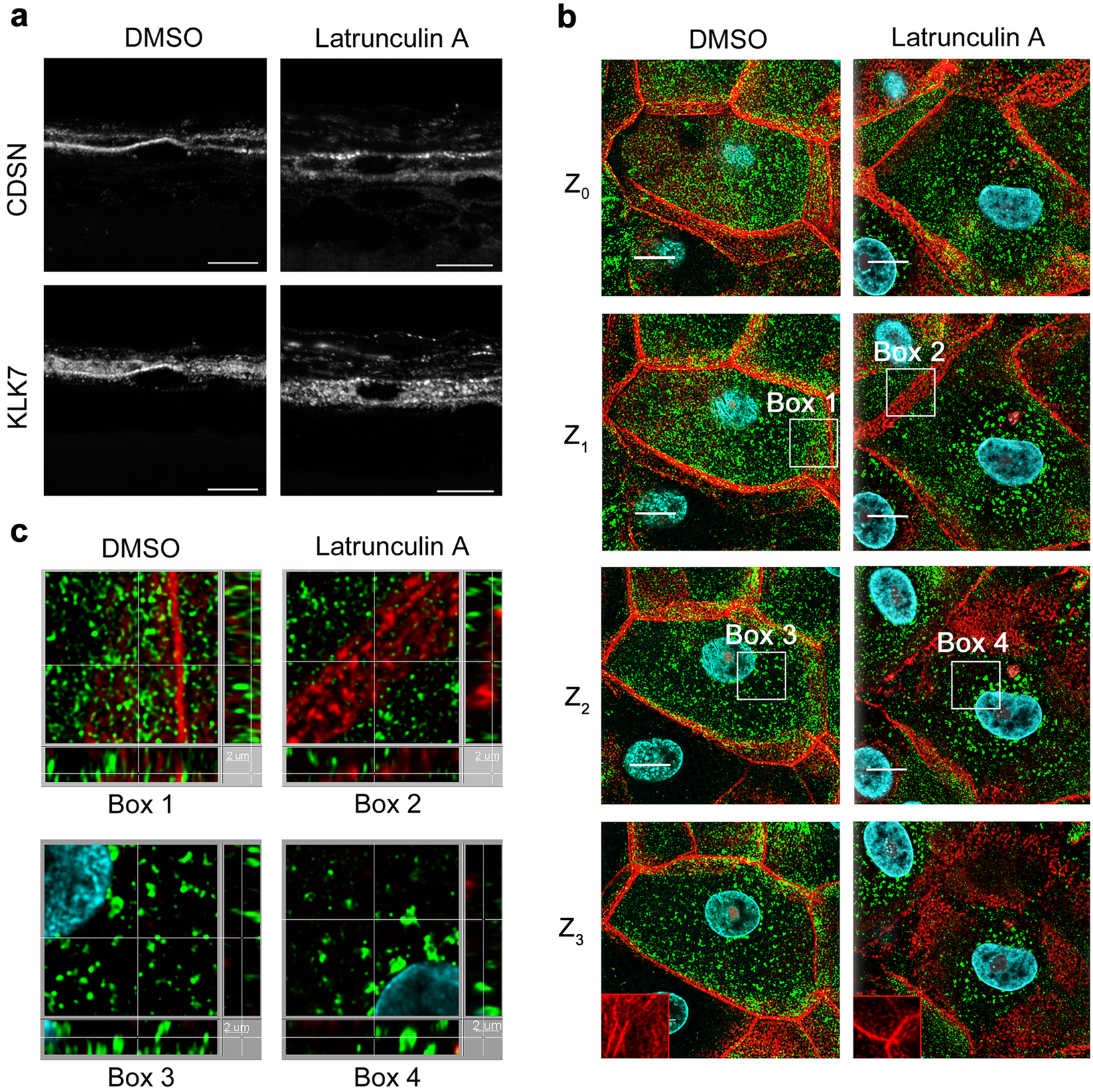
a
DMSO
Latrunculin A
CDSN
KLK7
b
DMSO
Latrunculin A
Z0
Z1
Z2
Z3
Box 1
Box 2
Box 3
Box 4
c
DMSO
Latrunculin A
2 um
Box 1
Box 2
Box 3
Box 4

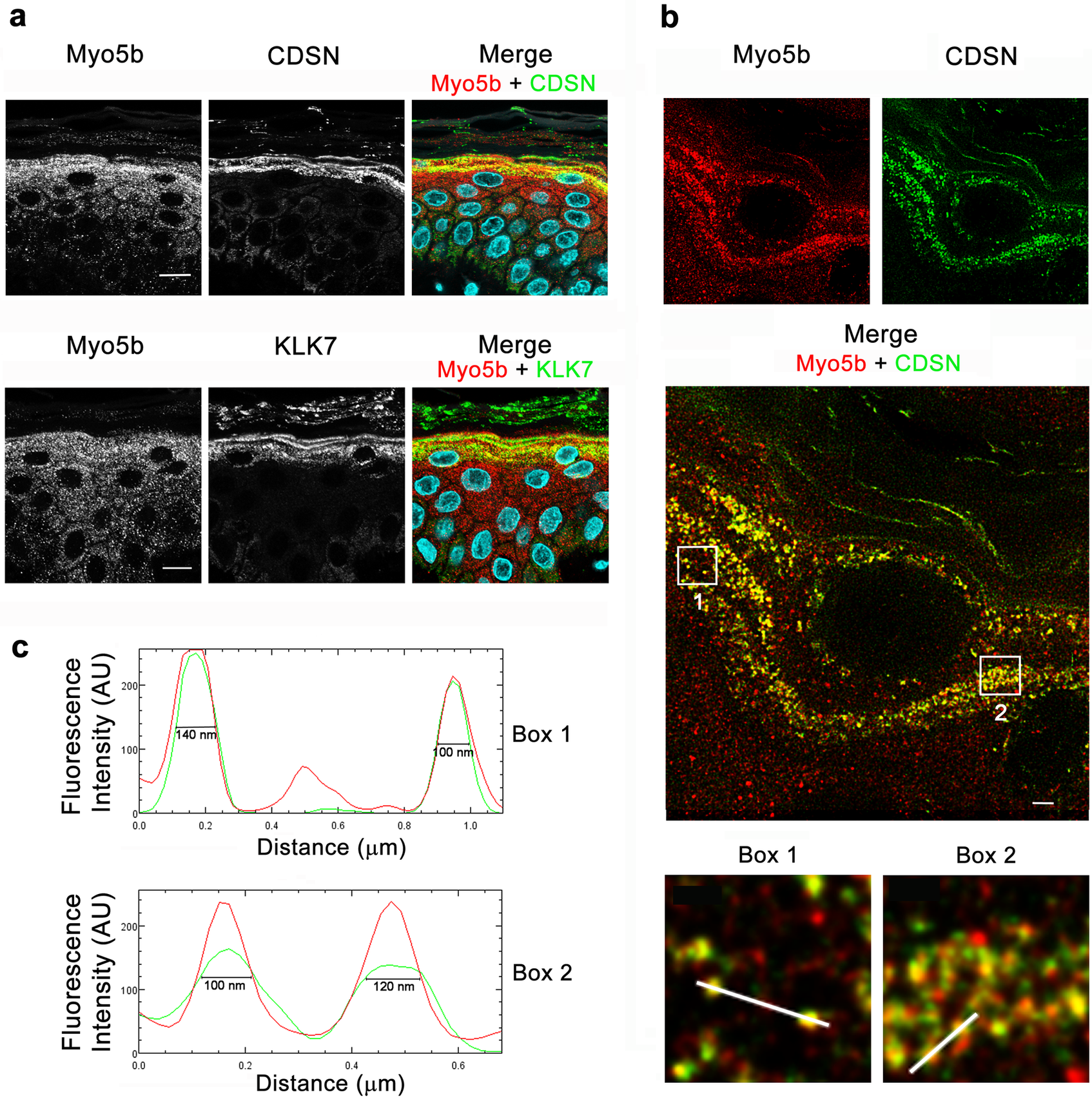
a
Myo5b
CDSN
Merge
Myo5b + CDSN
Myo5b
KLK7
Merge
Myo5b + KLK7
b
Myo5b
CDSN
Merge
Myo5b + CDSN
1
2
Box 1
Box 2
c
Fluorescence Intensity (AU)
140 nm
100 nm
Box 1
Distance (μm)
Fluorescence Intensity (AU)
100 nm
120 nm
Box 2
Distance (μm)

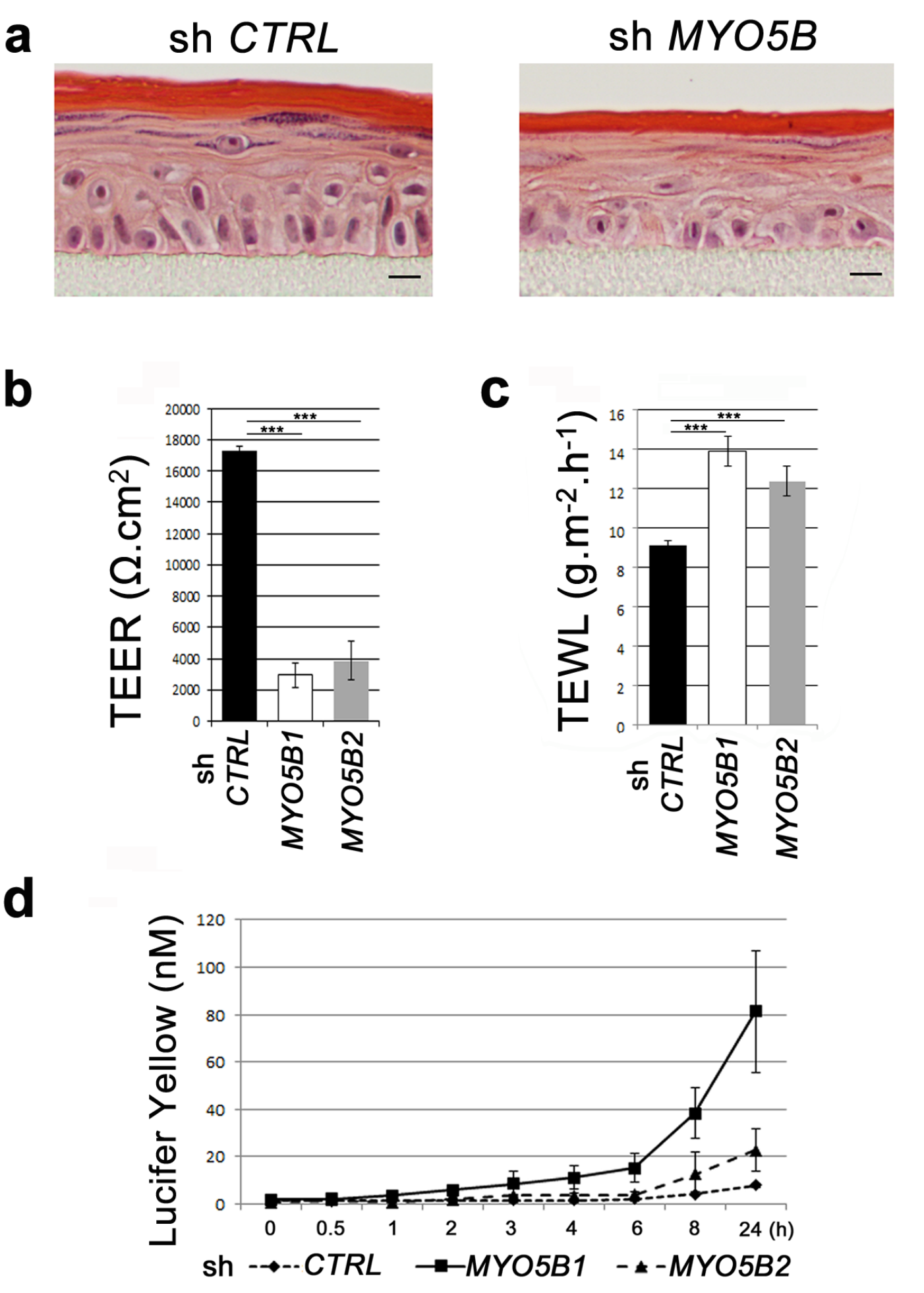
a
sh CTRL
sh MYO5B
b
TEER (Ω.cm²)
20000
18000
16000
14000
12000
10000
8000
6000
4000
2000
0
***
***
sh CTRL
MYO5B1
MYO5B2
c
TEWL (g.m-2.h-1)
16
14
12
10
8
6
4
2
0
***
***
sh CTRL
MYO5B1
MYO5B2
d
Lucifer Yellow (nM)
120
100
80
60
40
20
0
0
0.5
1
2
3
4
6
8
24 (h)
sh CTRL
MYO5B1
MYO5B2

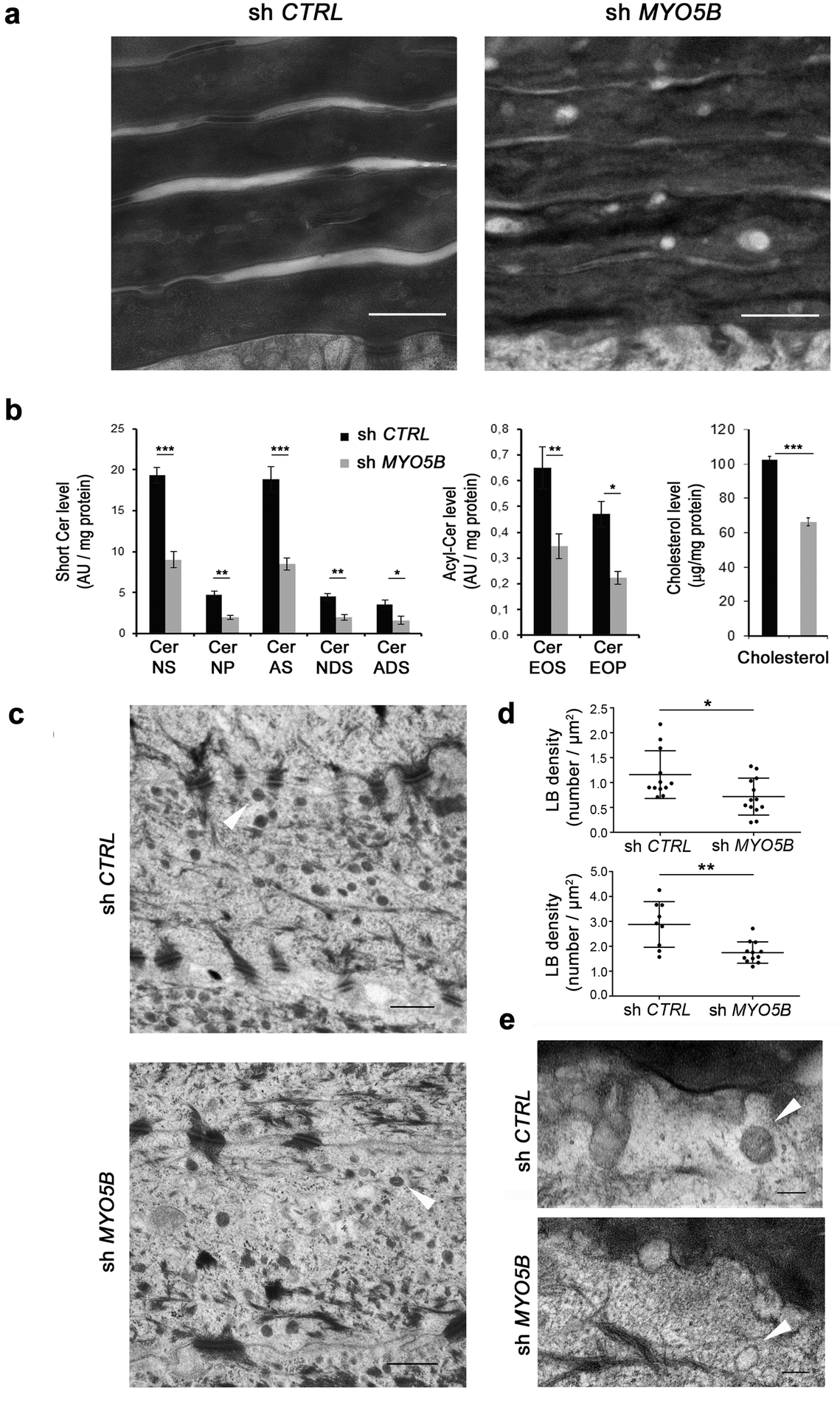
a
sh CTRL
sh MYO5B
b
sh CTRL
sh MYO5B
Short Cer level (AU / mg protein)
Cer NS
Cer NP
Cer AS
Cer NDS
Cer ADS
Acyl-Cer level (AU / mg protein)
Cer EOS
Cer EOP
Cholesterol level (µg/mg protein)
Cholesterol
c
sh CTRL
sh MYO5B
d
LB density (number / µm²)
sh CTRL
sh MYO5B
e
sh CTRL
sh MYO5B

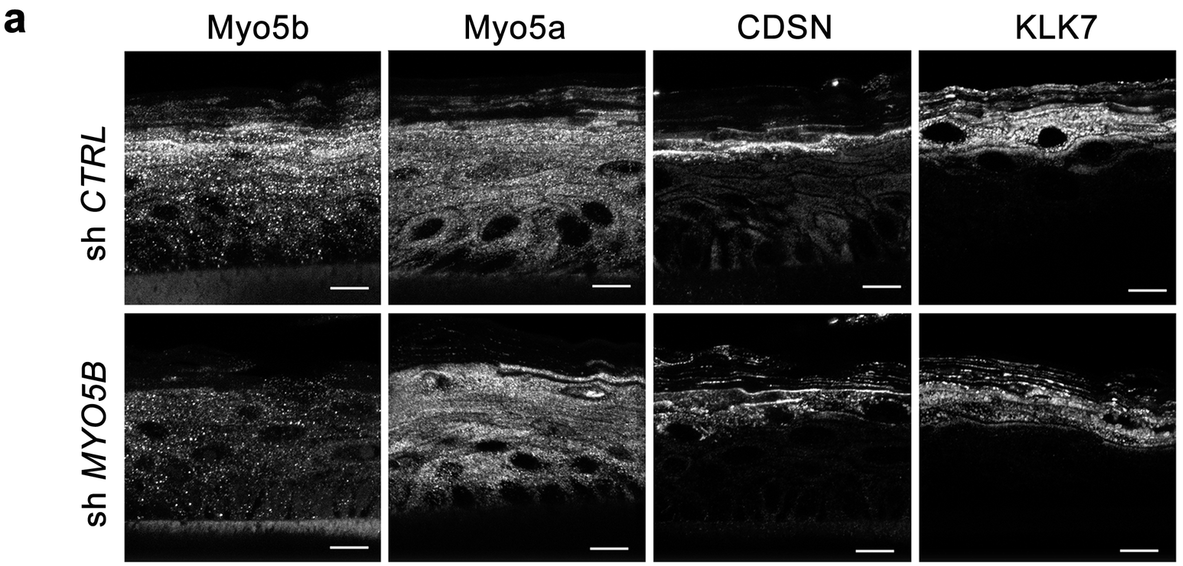
a
Myo5b
Myo5a
CDSN
KLK7
sh CTRL
sh MYO5B

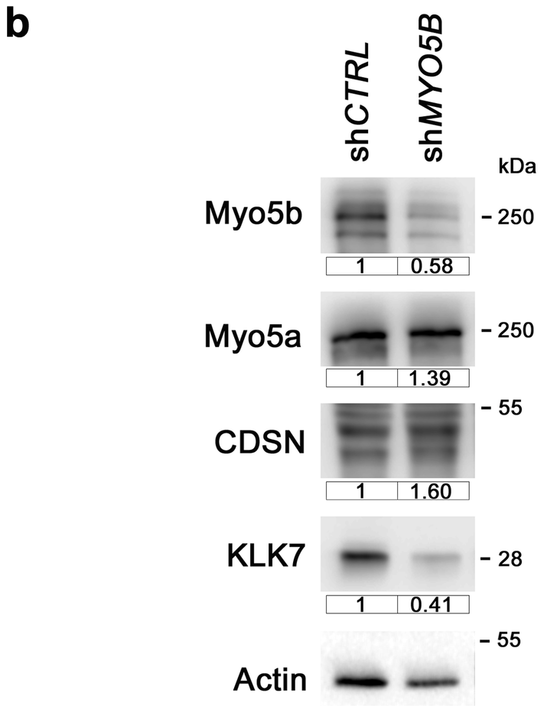
b
shCTRL
shMYO5B
kDa
Myo5b
250
1
0.58
Myo5a
250
1
1.39
CDSN
55
1
1.60
KLK7
28
1
0.41
Actin
55

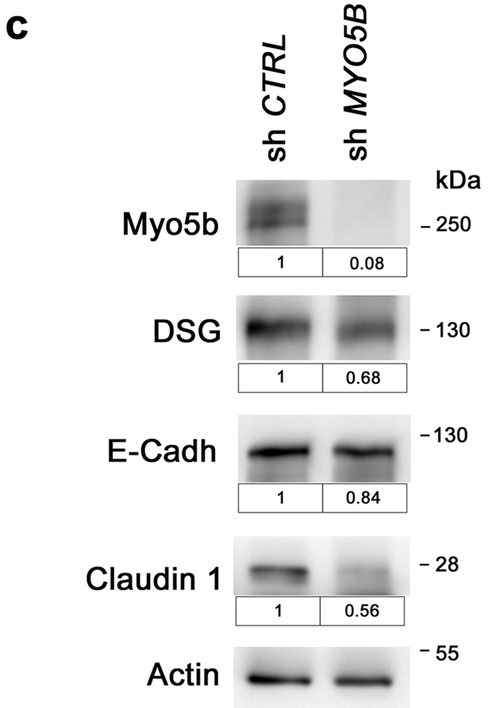
c
sh CTRL
sh MYO5B
kDa
Myo5b
250
1
0.08
DSG
130
1
0.68
E-Cadh
130
1
0.84
Claudin 1
28
1
0.56
Actin
55

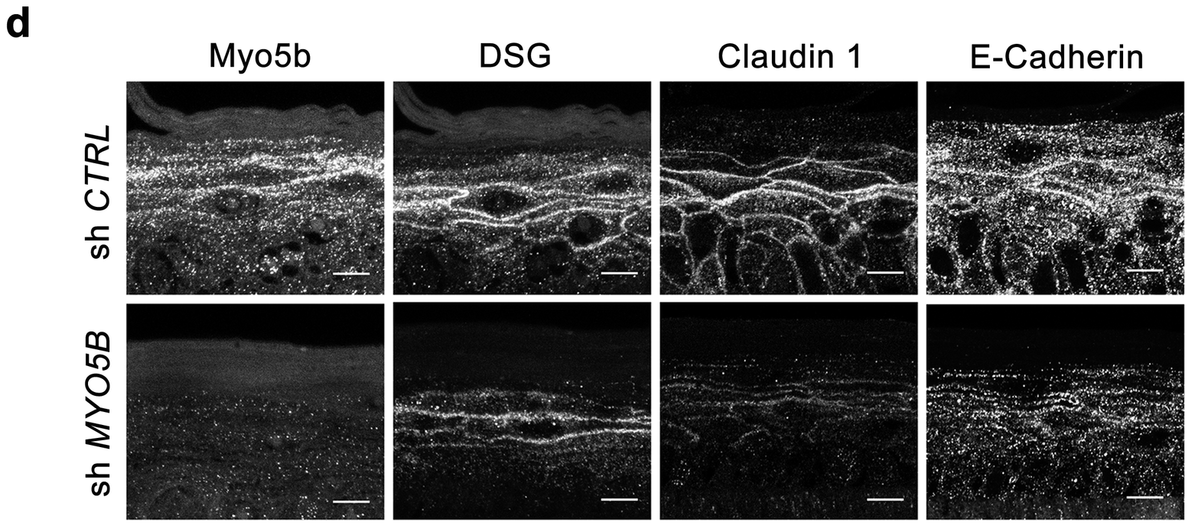
d
Myo5b
DSG
Claudin 1
E-Cadherin
sh CTRL
sh MYO5B